Effects of organized mesoscale heating on the MJO and precipitation in E3SMv1

C.-C. Chen[1], J. H. Richter[1], C. Liu[2], M. W. Moncrieff[1], Q. Tang[3], W. Lin[4], S. Xie[3] and P. J. Rasch[5]

[1] Climate and Global Dynamics Division, National Center for Atmospheric Research, Boulder, CO

[2] Research Applications Laboratory, National Center for Atmospheric Research, Boulder, CO

[3] Lawrence Livermore National Laboratory, Livermore, CA

[4] Brookhaven National Laboratory, Upton, NY

[5] Pacific Northwest National Laboratory, Richland, WA

Key Points:

- Multiscale Coherent Structure Parameterization (MCSP) was implemented in E3SMv1
- MCSP improves MJO and enhances Kelvin waves in E3SMv1
- Tropical precipitation biases are significantly reduced

Corresponding author: C.-C.Chen, cchen@ucar.edu

Abstract

Mesoscale organization of convection is typically not represented in global circulation models, and hence its influence on the global circulation is not accounted for. A parameterization aiming at representing the dynamical and physical effects of the circulation associated with organized convection, referred to as the multiscale coherent structure parameterization (MCSP), is implemented in the Energy Exascale Earth System Model version 1 (E3SMv1). Simulations are conducted to assess its impact on the simulated climate. Besides E3SMv1 simulations, we performed high-resolution (1 km) simulations using the Weather Research and Forecasting (WRF) Model to determine the temperature tendencies induced by mesoscale convective systems embedded in deep convection. We tuned the free parameters of the MCSP based on the WRF simulations. We found that the MCSP enhances Kevin wave spectra in E3SMv1, improves the representation of the Madden-Julian Oscillation, and reduces model precipitation biases over the tropical Pacific.

1 Introduction

The transport and mixing of heat and momentum throughout the atmosphere largely control the global circulation, and hence moisture and precipitation patterns. However, several transport processes occur on scales much smaller than a global circulation model (GCM) grid box, and hence have to be parameterized. Improvements in the representation of subgrid heat and momentum transport can lead to significant model improvements in the representation of wind stresses, moisture and precipitation patterns, and organized modes of variability [Richter and Rasch 2008]. In particular, convection is a large source of heat and momentum transport in the atmosphere, both on scales of individual convective plumes, as well as on scales of the order of 10-1000 km (mesoscales) [Moncrieff 1995, Houze 2004].

The importance of convective organization on the global circulation has been recognized for more than three decades but parameterizations of the attendant processes are missing from GCMs. Contemporary convective parameterizations commonly use a convective plume model (or a spectrum of plumes) [Arakawa and Schubert 1974, Kain et al. 1990, D'Andrea et al. 2014, Chen and Mapes 2018]. This is appropriate for unorganized convection. However, the assumption of a gap between the cumulus scale and the large-scale motion that underpins contemporary convective parameterizations fails to recognize mesoscale dynamics manifested in squall lines, mesoscale convective systems (MCS), mesoscale convective complexes (MCC), and multi-scale cloud systems associated with the Madden-Julian Oscillation (MJO). Over 50% of convective precipitation in the tropics is provided by MCS

defined as heavily precipitating closely coupled cumulus ensembles embedded in the more moderately precipitating stratiform regions of these systems [Nesbitt et al. 2006, Tao and Moncrieff 2009].

Mesoscale convective organization significantly modulates the life-cycle of moist convection, the transport of heat, moisture, momentum and chemical constituents [Houze 2004, Houze 2014]. Organized convection is abundant in environments featuring vertical wind shear and is typically associated with counter-gradient momentum transport [Moncrieff 1992]. Moncrieff and Liu [2006] designed a hybrid "predictor-corrector" framework to parameterize mesoscale convective systems and tested this approach in the Weather Research and Forecasting (WRF) model with a 60 km grid over the United States continent in summertime meteorological conditions. Specifically, a cumulus parameterization scheme gives the convective heating profile (predictor) which is then adjusted by adding sine-like upper-tropospheric warming and low-tropospheric cooling (i.e. 2nd baroclinic normal mode) heating corrector that emulates the mesoscale heating profile associated with MCSs. Moncrieff, Liu and Bogenschutz [2017] (hereafter MLB17) recently implemented a similar approach using the Community Atmosphere MOdel (CAM) in the form of multiscale coherent structure parameterization (MCSP) where organized convection is treated as coherent structures in a turbulent environment. MCSP is approximated by a slantwise layer overturning dynamical model that exchanges tropospheric layers via convectively generated mesoscale circulations (Fig. 1). Because slantwise layer overturning is not represented by existing convective parameterizations in a GCM, it is thus appropriate to simply add the "missing" mesoscale tendencies to traditional convective parameterizations. It follows that, for the first time, the difference between GCM simulations with and without MCSP can directly measure the large-scale effects of convective organization.

The implementation of MCSP was shown in MLB17 to improve precipitation biases in CAM version 5.5 (CAM5.5), e.g., in the tropical west Pacific (TWP), equatorial Africa, and the Inter Tropical Convergence Zone (ITCZ). MCSP also increased the Kelvin wave amplitude and extended the MJO signal from zonal wavenumber 1 to a more realistic wavenumber 1 - 5 range (MLB17).

The Energy Exascale Earth System Model, version 1 (E3SMv1) is a new Earth system model designed to meet the science needs of the nation and the mission of the Department of Energy (DOE). E3SM currently does not represent heat or momentum transport associated with mesoscale convective organization, so implementation of the MCSP introduces missing physical processes and can potentially reduce E3SM's biases, in particular, over the ITCZ, south Pacific convergence zone, and the maritime continent. Parameterization of mesoscale momentum transport is needed for horizontal resolutions of 25

km or coarser, which are the resolutions to be used by next generations of E3SM for its low-resolution science applications.

2 Mesoscale Heating Parameterization

To account for the impact of multiscale convective systems, their induced heating is added to the existing deep convection parameterization. Following Moncrieff and Liu [2006] and Moncrieff et al. [2017], mesoscale heating in the stratiform region is represented simply as a 2nd baroclinic normal mode with amplitude proportional to the vertically averaged convective heating provided by the convective parameterization. While a realistic vertical distribution of mesoscale heating is considerably more complex [Moncrieff 1992], this simplification captures its dominant features.

Figure 2b illustrates the vertical profile of mesoscale heating, which is dominated by heating (H) in the trailing stratiform region and evaporative cooling (C) beneath. In the Moncrieff and Liu (2006) prototype, the simplest possible vertical profile of mesoscale heating in Fig. 2, is given by the following equations:

$$\square\square(\square,\square) = -\square\square\square(\square)\,\square\square\square\left[2\square\frac{(\square-\square\square)}{(\square\square-\square\square)}\right] \quad (1)$$

$$\square* = \frac{\square\square+\square\square-}{2} \quad (2)$$

$$\square\square(\square) = \frac{1}{(\square\square-\square\square)}\int_{\square\square}^{\square\square}\square(\square)\square\square \quad (3)$$

where α is positive and is a free (tunable) parameter; ps and pt are the bottom and top of the convection respectively; p* is the location where the heating profile crosses the zero line; Qc is the average heating rate from the deep convection scheme.

3 WRF Simulations

We utilize version 4.0.3 of Weather and Research Forecasting model [Skamarock et al. 2008] (hereafter WRF) to carry out convection resolving simulations that will help to guide the free parameters in the mesoscale heating parameterization. WRF is a fully compressible, nonhydrostatic model with a terrain-following mass coordinate, suitable for use in a broad spectrum of applications across scales ranging from meters to thousands of kilometers. The computational domain is 4600 km x 1700 km at 2 km grid spacing with 65 stretched vertical levels and model top at 25 hPa. The employed subgrid

parameterizations included the WRF single-moment 6-class microphysics [Hong and Lim 2006], the YSU planetary boundary layer parameterization [Hong et al. 2006], the Noah-MP land surface model [Niu et al. 2011], and the Rapid Radiative Transfer Model (RRTMG) for longwave and shortwave atmospheric radiative fluxes [Iacono et al. 2008]. Spectral nudging was applied to wind and water vapor fields above the planetary boundary layer to preserve the characteristics of large-scale circulation, while allowing the development of sub-synoptic, mesoscale and convective processes. Two multi-day episodes of active convection associated with an MJO event (MLB17) were selected for experimentation, corresponding to a 9-day convective period in the Indian Ocean (Fig. 3a) and a 14-day convective period in the western Pacific (Fig. 4a), respectively. The hourly, 31-km-resolution ERA5 reanalysis data provided initial and boundary conditions. It is seen from Figs. 3b and 4b that the observed convective systems are well captured in the WRF convection resolving simulations in both the Indian Ocean and the western Pacifc. Therefore, the WRF simulations over these two selected periods provide useful information to guide the selection of the free parameter α in MCSP for its GCM applications.

An algorithm of convective-stratiform separation in radar data analysis was adopted for convective-stratiform heating partitioning. As detailed in Steiner et al. [1995] and Houze [2014], the procedure is to first identify convective area, and then the remaining part of a studied area is treated as stratiform region. The philosophy for determining convective region is based on the intensity and peakness criteria in the reflectivity field. Specifically, any grid point either with at least 40dBZ or exceeding the surrounding background reflectivity by a specified factor is considered a convective center. Additionally, grid points surrounding a convective center, as described in Steiner et al. [1995], are considered a convective area. A caveat of this approach is its inability to identify a shallow convective area.

By using the aforementioned algorithm to analyze the WRF simulations conducted, the convective-stratiform heating partitioning is obtained. As illustrated in Fig. 5, it is found that shallow stratiform heating is approximately 0.3 to 0.5 that of the deep convective heating in both Indian Ocean and the western Pacific. Therefore, αin Eq. 1 is assumed to be 0.3 and 0.5 in this study.

Since a favorable condition for the development of MCS includes substantial vertical wind shear, we add a wind shear threshold in order to determine where MCSP is triggered. To examine the sensitivity of the simulated climate on the wind shear threshold, we performed simulations with the zonal wind shear between surface and 600 hPa set to exceed 0, 3, 5, and 7.5 m/s as the trigger. This condition ensures that MCSP does not alter convective activities where the possibility of MCS formation is low. This is an update to the formulation of MLB17.

4 Climate Model Simulations

a) Model Description

The climate model employed in this study is the Energy Exascale System Model, version 1 (E3SMv1) [Golaz et al., 2019], which originated from the Community Earth System Model version 1 (CESM1). There are significant developments in all individual components of the model compared to CESM1 including: 1) new options for representing soil hydrology and biogeochemistry in the land model (ELM) based on the Community Land Model version 4.5 (CLM4.5), 2) new ocean and sea-ice components based on the Model for Prediction Across Scales (MPAS) framework, and 3) a new river model (i.e., Model for Scale Adaptive River Transport (MOSART)) that has not been previously used in a coupled Earth System Model.

Several updates to the atmospheric component of E3SMv1, EAMv1, are built upon the Community Atmosphere Model version 5.3 (CAM5.3). EAMv1 employs a unified treatment of planetary boundary layer turbulence, shallow convective, and cloud macrophysics with a third-order turbulence closure parameterization (CLUBB; Cloud Layers Unified by Binormals) [Golaz et al., 2002; Larson and Golaz, 2005; Larson, 2017] which eliminates unrealistic separation of these physical processes. Turbulence, clouds, and convective processes are handled by the Zhang and McFarlane (ZM) deep convection scheme [Zhang and McFarlane, 1995] paired with CLUBB and an updated cloud microphysical scheme, version 2 of Morrison and Gettelman (MG2) [Morrison and Gettelman, 2008; Gettleman and Morrison, 2015; Gettelman et al., 2015]. An update to the MG2 is a Classical Nucleation Theory (CNT) based on ice nucleation (IN) parameterization for heterogeneous ice formation in mixed phase clouds [Wang et al., 2014]. Rasch et al. [2019] provide an overview of EAMv1,while Xie et. al. [2018], Qian et al. [2018], and Zhang et al. [2019] show simulated cloud and convective characteristics and the rationale for model tuning and Tang et al. [2019] documents its regionally refined capability for developing high-resolution physics parameterizations.

The horizontal resolution of the simulations is ~100 km and there are 72 vertical levels with the model top at 60 km. The configuration of the vertical grid is shown in Fig. 1 of Xie et al. [2018] with vertical spacing in the upper troposphere and lower stratosphere ~600 m.

b) Simulations

We carried out six simulations with the stand alone atmospheric component of E3SM (EAMv1) with prescribed observed sea-surface temperatures and sea-ice concentrations (‘AMIP’ simulations) and

four simulations with the fully coupled version of E3SMv1 ('Coupled' simulations). All simulations are 30 years, beginning in November 1980 and ending in December 2009.

In these simulations we vary the parameter alpha (□) as well as the wind shear trigger (tunable parameters). The simulations are summarized in Table 1.

Table 1: Experimental set-up. All simulations are 30 years long from 1980 to 2009.

	Simulation Type	□	Wind shear trigger (m/s)
EAMv1	AMIP	0	0
EAMv1_a300	AMIP	0.3	0
EAMv1_a500	AMIP	0.5	0
EAMv1_a530	AMIP	0.5	3
EAMv1_a550	AMIP	0.5	5
EAMv1_a575	AMIP	0.5	7.5
E3SMv1	Coupled	0	0
E3SMv1_a300	Coupled	0.3	0
E3SMv1_a500	Coupled	0.5	0
E3SMv1_a530	Coupled	0.5	3

c) Results

We document the most significant impacts to EAMv1/E3SMv1 simulations due to MCSP as follows.

(i) Deep Convection

The heating rate of MCSP and its impact on the deep convection scheme are illustrated in Fig. 6. As shown in Fig. 2b, when deep convection occurs, the circulation of MCSs induces lower-tropospheric cooling and upper-tropospheric warming. The amplitude of MCSP heating alone is illustrated in Fig 6a for □=0.3 and □=0.5. With □=0.3 (□ = 0.5) the lower tropospheric cooling peaks at 0.7 K/day (1.2 K/day), where as the mid-tropospheric heating peaks at 0.25 K/day (0.5 K/day). MCSP produces temperature tendencies in the EAMv1 simulations that reflect the impact of MCSs. However, it is important to note that the heating tendencies illustrated in Fig. 6a are averaged per occurrence of deep

convection. Thus, the asymmetry in the magnitude of cooling and heating tendencies in the vertical profile implies that there is more frequent occurrence of shallower convection which results in stronger averaged cooling in the lower troposphere. Also notice that MCSP, by design, has a zero vertically integrated temperature (dry static energy) tendency as a correction term is added to the column to ensure the parameterization conserve total energy, and thus there is shallower but more intense cooling in the lower troposphere and deeper and weaker warming in the upper troposphere.

The heating rate from the Zhang and McFarlane (ZM) [Zhang and McFarlane 1995] deep convection scheme, with and without MCSP included, is shown in Fig. 6b. With the addition of MCSP, the ZM heating rate is weaker in the lower troposphere because MCSP cools the lower troposphere. However, the heating rate in the upper troposphere is also weaker than the control simulation where MCSP adds heating (as will be explained below). Moreover, with a larger □ the heating rate becomes weaker in the upper troposphere which is somewhat surprising since MCSP provides a heating tendency.

The implication of the circulation associated with MCSs is to stabilize the troposphere since it has a cooling effect in the lower troposphere and a heating effect aloft. Thus, when deep convection occurs, MCSP reduces convective available potential energy (CAPE) by enhancing the tropospheric stability making convection less persistent and less frequent. Hence, the additional MCSP heating has a destabilizing effect leading to reduced deep convection, and reduced ZM heating. With a larger □, the weakening of the heating rate by the deep convection scheme is more pronounced.

(ii) Tropical Variability

One well documented bias in E3SMv1 is the representation of tropical variability. In particular, the Kelvin waves are much weaker than observations [Richter et al. 2019, Rasch et al. 2019]. As described in Richter et. al [2014], Kelvin waves are an important driver of the quasi-biennial oscillation (QBO). As illustrated in Fig 7b, the baseline model of EAMv1 indeed simulates much weaker Kelvin waves than TRMM observations (Fig. 7a).

Importantly, MCSP enhances the Kelvin wave spectra in all simulations. The most pronounced increase in Kelvin wave activity occurs when there is no wind shear trigger threshold in MCSP so it gets activated whenever deep convection occurs. With a wind shear trigger, MCSP is activated less frequently and therefore has a weaker impact on the simulation.

(iii) MJO

The MJO is a dominant mode of subseasonal variability in the tropics. The key signature of MJO is eastward propagation of tropical convection originating from the Indian Ocean to the west Pacific during the boreal winter [Madden and Julian 1971; Madden and Julian 1972]. The MJO is often not well represented in climate models [Ahn et al. 2017; Ahn et al. 2020]. In observations, the cross-lag correlation of precipitation shows pronounced eastward propagation from 60E to 160E and meridional propagation from the equator to 20S and 20N (Fig. 8a).

The cross-lag correlation, of precipitation and zonal wind at 850 hP, indicates that the baseline EAMv1 produces substantial westward precipitation (top panel of Fig. 8b) instead of eastward propagation (top panel of Fig. 8a) in the Indian Ocean basin from the ERA-Interim reanalysis.This indicates that there is substantial westward propagation component in the baseline model. The observation indicates that there is nearly symmetrical meridional propagation, extending to 20 S/N from the equator in precipitation (bottom panel of Fig. 8a). However, EAMv1 simulates much less meridional propagation in the Indian Ocean basin (bottom panel of Fig. 8b).

With MCSP, EAMv1 simulates less westward propagation and more meridional propagation (Fig 8b c-g). The setup with = 0.5 and wind shear threshold = 3 m/s (Fig. 8e) shows significant improvement over the baseline model since the simulation shows the clearest eastward propagation in precipitation.

When run in the fully coupled configuration (E3SMv1), the model shows significant improvement over EAMv1 in simulating the MJO. The fully coupled model produces clear eastward propagation of precipitation in the Indian Ocean basin (Fig. 9a) and removes most of the westward propagation occuring in EAMv1 (Fig. 8b). However, meridional precipitation propagation in E3SMv1 is still weak compared to observation. With inclusion of MCSP, the eastward precipitation propagation is faster than the baseline E3SMv1 (Fig. 9b) when = 0.5 (Fig. 9c,d). MCSP also extends meridional propagation farther from the equator.

The spectral characteristics of the MJO are considered in Figures 10 and 11. Observations (Fig. 10a) show eastward propagation in outgoing longwave radiation (OLR) in the Indian Ocean with a period between 30 and 90 days and wave numbers between 1 and 3 during the boreal winter. The baseline EAMv1 has little power between 30 and 90 days in eastward propagation (Fig, 10b) despite substantial eastward propagation for periods greater than 90 days. In addition, there is slow (>90 days) westward

propagation in the baseline model.

When MCSP is included in EAMv1, slow (>90 days) eastward propagation of OLR is further enhanced (Fig. 10 c-g). However, more power within the window of 30-90 days in eastward propagation is evident in Fig. 10 c-e, implying that the simulated MJO is improved. It is worth noting that Fig. 10e shows much stronger westward propagation which indicates degradation from the baseline model simulation.

E3SMv1 indicates an improved MJO compared to EAMv1 in terms of increased power within the window of 30-90 days in eastward propagation as shown in Fig. 11a, although the eastward propagation is still too slow compared to observation (Fig. 10a). With MCSP, the fully coupled model simulations (Fig. 11b-d) show further improvements, i.e., increased power in the 30-90 day window in eastward propagation whilst not enhancing westward propagation. The MJO spectra is too strong for □ = 0.5 without a wind shear threshold (Fig.11c), but is reduced by a wind shear trigger threshold of 3 m/s (Fig. 11d).

Figure 12 illustrates the life-cycle composite of MJO revealing that EAMv1 simulates much weaker OLR (Fig. 12 b). With MCSP, the intensity of OLR is enhanced slightly but still much weaker than observation. Additionally, EAMv1, without or with MCSP, also lacks organized convection within the Indian Ocean basin during phases 2 and 3, compared to observation (Fig. 12a).

Figure 13a shows E3SMv1 simulates stronger OLR, but the lack of organized convection in the Indian Ocean basin during phases 2 and 3 still persists. With MCSP (Fig. 13b,c,d) , the intensity of OLR is stronger, mainly in the later phases (5-8) but the model also fails to produce strong organized convection in the Indian Ocean basin during phases 2 and 3.

(iv) Precipitation Biases

Since MCSP is implemented within the deep convection scheme, it is anticipated to alter convective precipitation especially in the lower latitudes where active deep convection is extensive. Indeed, MCSP mainly modifies precipitation near the tropics and subtropics in both EAMv1 (Fig. 14) and E3SMv1 (Fig.15). In both model configurations, MCSP robustly reduces precipitation around the tropical east Pacific, Colombia, and Ecuador (see Fig. 14, 15). The reduction of precipitation in these regions is more pronounced when the wind shear threshold is set smaller, meaning that MCSP is triggered more frequently. Also, these regions are where the baseline EAMv1/E3SMv1 produces positive biases in precipitation so MCSP provides an improvement. Nevertheless, the reduction is weaker during

December-January-February (DJF), a feature also evident in CAM5.5 simulations, i.e. Fig. 14b of MLB17.

The annual average of the EAMv1 simulations with MCSP shares several other features found in CAM5.5 (e.g., Fig. 14b in MLB17), such as enhancement in precipitation in the tropical west Pacific, south China sea, and Indian Ocean basin, and reduction in tropical Africa (see Fig. 14d). Such features are suppressed with a higher wind shear trigger (Fig. 14 b,c). It is also worth noting that the enhancement in precipitation in south China sea and the Indian Ocean is mainly attributed to DJF (Figs. 14 g,h) since in June-July-August (JJA, see Figs. 14 k,l), the change in precipitation in these regions due to MCSP is negative. However, these features represent a degradation to EAMv1 because the baseline model already simulates positive biases in precipitation in these regions (Fig. 14a).

Another region seen significant change in precipitation due to MCSP is in south and southeast Asia, and over India and Indian Ocean basin. In DJF, a reduction in precipitation due to MCSP is found (Fig. 14j,k,l and Fig. 15j,k,l). EAMv1 and E3SMv1 in the baseline model configuration both produce positive biases in these regions and thus such changes in DJF make the simulated climate closer to observation.

When MCSP is incorporated in the fully coupled model, E3SMv1, the change in precipitation in the tropical west Pacific differs from those in EAMv1. For the annual average, a reduction in precipitation occurs (Figs. 15 b,c,d), which improves the model biases. However, E3SMv1 with MCSP simulates more precipitation in these regions in DJF (Figs. 15 f,g,h) and thus degrades the model. The reduction in annual precipitation is thus attributed to more pronounced lower precipitation simulated in JJA (Figs. 15 j,k,l).

In terms of annual precipitation, MCSP does not induce a coherent feature in the tropical west Pacific between EAMv1 and E3SMv1. However, the parameterization induces the same features in seasonal averages: MCSP enhances precipitation in DJF but reduces precipitation in JJA in these regions.

5 Summary and Conclusions

We implemented MCSP in E3SMv1 with modifications from its original form and investigated its impact on the simulated climate in AMIP and coupled simulations. MCSP represents the important organized physical and dynamical processes induced by the MCS circulation in the form of lower-tropospheric cooling and upper-troposphere heating. The intensity of the cooling and heating is

proportional to the column integral of heating by deep convection revealed by convection resolving WRF simulations. Specifically, when deep convection occurs, MCSP decreases the convective available potential energy by enhancing the tropospheric static stability, acting to suppress subsequent convection .

Modeling efforts have attempted to improve the simulated MJO in climate models in recent years. Implementation of MCSP in E3SMv1 provides significant improvement in MJO simulation in terms of stronger eastward propagation of precipitation and OLR in the Indian Ocean basin and increased power in the eastward spectra for periods between 30 and 90 days. This suggests that convection over this region, as simulated by the baseline model, is over-persistent and hinders propagation. Since MCSP stabilizes the troposphere when deep convection occurs, it shortens the duration of convection within a grid-cell and helps the persistent propagation of coherent convective systems.

In the simulated climate, MCSP reduces precipitation over the tropical western Pacific, Colombia, and Ecuador, where the baseline model simulates too much precipitation. This feature is independent of the model configurations and implies that the baseline model may have too-persistent deep convection in these regions. With MCSP removing some CAPE, it may serve to improve precipitation biases where deep convection is overly active in the baseline model.

Under the two model configurations examined in this study, different model behavior was found in the annual precipitation around tropical west Pacific induced by MCSP: EAMv1 simulated higher precipitation but E3SMv1 simulated lower precipitation. In further analysis, we found that MCSP enhanced precipitation in these regions in DJF and reduced precipitation in JJA. This signature was not dependent on the model configuration. Thus, it is evidently crucial to analyze the seasonal impact of MCSP instead of focusing on only the annual average since its impact can reverse sign depending on the season.

Herein we limited the scope of our investigation to the effects of mesoscale convective heating as represented by MCSP on the simulated global climate. However, momentum transport is another important feature of organized moist convection that requires investigation. Note that, in an atmosphere-only model connext, MLB17 compared the effects of MCSP convective heating and convective momentum transport and discovered interesting differences in a global context. In our future MCSP work, we will explore and compare the effects of convective momentum transport and convective heating in the atmosphere-only and coupled versions of E3SM.

Acknowledgements:

This research was supported by DOE's Office of Biological and Environmental Research (BER), Earth and Environmental System Modeling program and the Energy Exascale Earth System Model (E3SM) project for its next generation of development (NGD) of atmospheric physics, funded by the DOE, Office of Science, BER. This research used resources of the National Energy Research Scientific Computing Center, a DOE Office of Science User Facility supported by the Office of Science of the U.S. DOE under Contract No. DE-AC02-05CH11231. This material is based upon work supported by the National Center for Atmospheric Research, which is a major facility sponsored by the National Science Foundation under Cooperative Agreement No. 1852977. Work at LLNL was performed under the auspices of the U.S. DOE by Lawrence Livermore National Laboratory under contract DE-AC52-07NA27344. The Pacific Northwest National Laboratory is operated for the U.S. DOE by Battelle Memorial Institute under contract DE-AC05-76RL01830. Output from the default E3SMv1 simulations can be downloaded via the following link: https://portal.nersc.gov/project/e3sm/cchen24/MCSP_JAMES/

References

Ahn, M.-S., Kim, D., Sperber, K.R., Kang, I.-S., Maloney, E., Waliser, D., and Hendon, H., 2017: MJO simulation in CMIP5 climate models: MJO skill metrics and process-oriented diagnosis. *Clim Dyn* 49, 4023–4045, https://doi.org/10.1007/s00382-017-3558-4

Ahn, M.-S., Kim, D., Kang, D., Lee, J., Sperber, K. R., Gleckler, P. J., Jiang, X., Ham, Y.-G., and Kim, H., 2020: MJO propagation across the Maritime Continent: Are CMIP6 models better than CMIP5 models? *Geophy. Res. Lett.*, 47, e2020GL087250. https://doi.org/10.1029/2020GL087250

Chen, B., and B. E. Mapes, 2018: Effects of a simple convective organization scheme in a two-plume gcm. *J. Adv. Model Earth Syst.*, **10**(3):867–80.

D'Andrea, F, P. Gentine, A. K. Betts, B. R. Lintner, 2014:. Triggering deep convection with a probabilistic plume model. *J. Atmos. Sci.*, **71**:3881–901. https://doi.org/10.1175/JAS-D-13-0340.1.

Golaz, J.-C., P. M. Caldwell, L. P. Van Roekel, M. R. Petersen, Q. Tang, J. D. Wolfe, et al., 2019: The DOE E3SM coupled model version 1: Overview and evaluation at standard resolution. *Journal of Advances in Modeling Earth Systems*, **11**, 2089–2129. https://doi.org/10.1029/2018MS001603.

Golaz, J.-C., V. E. Larson, and W. R. Cotton, 2002: On a PDF-based model for boundary layer clouds. Part I: Method and model description. *J. Atmos. Sci.*, **59**(24), 3540–3551.

Hong, S. and Lim, J., 2006: The WRF single-moment 6-class microphysics scheme (WSM6). *Journal of the Korean Meteorological Society*, **42**, 129-151.

Hong, S.-Y., Y. Noh, and J. Dudhia, 2006: A new vertical diffusion package with an explicit treatment of entrainment processes. *Mon. Wea. Rev.*, **134**, 2318–2341, doi:10.1175/MWR3199.1.

Houze, R. A., Jr., 2004: Mesoscale convective systems. *Rev. Geophys.*, **42**, RG4003, doi:10.1029/2004RG000150.

Houze, R. A., Jr., 2014: Cloud Dynamics. 2nd ed. *International Geophysics Series*, Vol. 14, Academic Press, 432 pp.

Gettelman, A., and H. Morrison, 2015: Advanced two-moment bulk microphysics for global models. Part I: Off-line tests and comparison with other schemes. *J. Climate*, **28**(3), 1268–1287. https://doi.org/10.1175/JCLI-D-14-00102.1.

Gettelman, A., H. Morrison, S. Santos, P. Bogenschutz, and P. M. Caldwell, 2015: Advanced two-moment bulk microphysics for global models. Part II: Global model solutions and aerosol-cloud interactions. *J. Climate*, **28**(3), 1288–1307.https://doi.org/10.1175/JCLI-D-14-00103.1

Iacono, M. J., J. S. Delamere, E. J. Mlawer, M. W. Shephard, S. A. Clough, and W. D. Collins, 2008: Radiative forcing by longlived greenhouse gases: Calculations with the AER radiative transfer models. *J. Geophys. Res.*, **113**, D13103, doi:10.1029/2008JD009944.

Larson, V. E., 2017: CLUBB-SILHS: A parameterization of subgrid variability in the atmosphere. ArXiv:1711.03675 [Physics].

Larson, V. E., and J. C. Golaz, 2005: Using probability density functions to derive consistent closure relationships among higher-order moments. *Mon. Wea. Rev.*, **133**(4), 1023–1042. https://doi.org/10.1175/MWR2902.1.

Madden, R. A., and Julian, P. R., 1971: Detection of a 40–50 day oscillation in the zonal wind in the tropical Pacific. Journal of the Atmospheric Sciences, 28(5), 702–708. https://doi.org/10.1175

Madden, R. A., and Julian, P. R., 1972: Description of global-scale circulation cells in the tropics with a 40–50 day period. Journal of the Atmospheric Sciences, 29(6), 1109–1123. https://doi.org/10.1175

Moncrieff, M.W., 1992: Organized convective systems: Archetypal models, mass and momentum flux theory, and parameterization. *Quart. J. Roy. Meteorol. Soc*, **118**, 819-850.

Moncrieff, M. W., 1995: Mesoscale convection from a large-scale perspective. *Atmos. Res.*, **35**, 87-112. https://doi.org/10.1016/0169-8095(94)00012-3

Moncrieff, M. W., and C. Liu, 2006: Representing convective organization in prediction models by a hybrid strategy. *J. Atmos. Sci.*, **63**, 3404–3420, doi:10.1175/JAS3812.1.

Moncrieff, M. W., C. Liu, and P.. Bogenschutz, 2017: Simulation, modeling, and dynamically based parameterization of organized tropical convection for global climate models. *J. Atmos. Sci.*, **74**, 1363-1380, doi:10.1175/JAS-D-16-0166.1.

Morrison, H., and A. Gettelman, 2008: A new two-moment bulk stratiform cloud microphysics scheme in the Community Atmosphere Model, version 3 (CAM3). Part I: Description and numerical tests. *J. Climate*, **21**(15), 3642–3659.

Nesbitt, S. W., R. Cifelli, and S. A. Rutledge, 2006: Storm morphology and rainfall characteristics of TRMM precipitation features, *Mon. Wea. Rev.*, **134**, 2702-2721, doi:10.1175/MWR3200.1.

Niu, G.-Y, Z.-L. Yang, K. E. Mitchell, F. Chen, M. B. Ek, M. Barlage, A. Kumar, K. Manning, D. Niyogi, E. Rosero, M. Tewari, and Y. Xia, 2011: The community Noah land surface model with multiparameterization options (Noah-MP): 1. Model description and evaluation with local-scale measurements. *J. Geophys. Res.*, **116**, D12109, doi: 10.1029/2010JD015139.

Qian, Y., H. Wan, B. Yang, J.-C. Golaz, B. Harrop, Z. Hou, et al., 2018: Parametric sensitivity and uncertainty quantification in the version 1 of E3SM atmosphere model based on short perturbed parameter ensemble simulations. *J. Geophys. Res*., **123**, 13,046–13,073. https://doi.org/10.1029/2018JD028927

Rasch, P. J., S. Xie, P.-L. Ma, W. Lin, H. Wang, Q. Tang, et al. (2019). An overview of the atmospheric component of the Energy Exascale Earth System Model. *Journal of Advances in Modeling Earth Systems*, **11**, 2377–2411. https://doi.org/10.1029/2019MS001629.

Richter, J. H., J. T. Bacmeister, and A. Solomon, 2014: On the simulation of the quasi-biennial oscillation in the Community Atmosphere Model, version 5. *J. Geophys. Res.*, **119**, 3045–3062. https://doi.org/10.1002/2013JD021122. Richter, J. H., C.-C. Chen, Q. Tang, S. Xie, and P. J. Rasch, 2019: Improved simulation of the QBO in E3SMv1. *Journal of Advances in Modeling Earth Systems*, **11**, 3403–3418. https://doi.org/10.1029/2019MS001763.

Richter, J. H., and P. J. Rasch, 2008: Effects of convective momentum transport on the Atmospheric Circulation Model , version 3. *J. Climate*, **21**, 1487-1499. Doi: 10.1175/2007JCLI1789.1

Skamarock, W. C., Klemp, J. B., Dudhia, J., Gill, D. O., Barker, D., Duda, M. G., and Powers, J. G., 2008: A description of the advanced research WRF Version 3, No. NCAR/TN-475+STR, University Corporation for Atmospheric Research, doi:10.5065/D68S4MVH.

Steiner, M., R. A. Houze Jr., and S. E. Yuter, 1995: Climatological characterization of three-dimensional storm structure from operational radar and rain gauge data. *J. Appl. Meteor.*, **34**, 1978–2007.

Tang, Q., Klein, S. A., Xie, S., Lin, W., Golaz, J.-C., Roesler, E. L., Taylor, M. A., Rasch, P. J., Bader, D. C., Berg, L. K., Caldwell, P., Giangrande, S. E., Neale, R. B.,

Qian, Y., Riihimaki, L. D., Zender, C. S., Zhang, Y., and Zheng, X.: Regionally refined test bed in E3SM atmosphere model version 1 (EAMv1) and applications for high-resolution modeling, Geosci. Model Dev., 12, 2679–2706, https://doi.org/10.5194/gmd-12-2679-2019, 2019.

Tao, W.-K., and M. W. Moncrieff, 2009: Multiscale cloud system modeling. *Rev. Geophys.*, **47**, RG4002, doi:10.1029/2008RG000276.

Wheeler, M. and G. Kiladis, 1999: Convectively coupled equatorial waves: analysis of clouds and temperature in the wavenumber-frequency domain. *J. Atmos. Sci.*, **56**(3): 374-300. https://doi.org/10.1175/1520-0469(1999)056<0374:CCEWAO>2.0.CO;2.

Xie, S., W. Lin, P. J. Rasch, P.-L. Ma, R. Neale, V. E. Larson, et al., 2018: Understanding cloud and convective characteristics in version 1 of the E3SM atmosphere model. *Journal of Advances in Modeling Earth Systems*, **10**, 2618–2644. https://doi.org/10.1029/2018MS001350.

Zhang, G. J., and N. A. McFarlane, 1995: Sensitivity of climate simulations to the parameterization of cumulus convection in the Canadian Climate Centre General Circulation Model. *Atmosphere-Ocean*, **3**, 407–446.

Zhang, Y., S. Xie, W. Lin, S. A. Klein, M. Zelinka, P.-L.Ma, et al., 2019: Evaluation of clouds in version 1 of the E3SM atmosphere model with satellite simulators. *Journal of Advances in Modeling Earth Systems*, **11**, 1253–1268. https://doi.org/10.1029/2018MS001562.

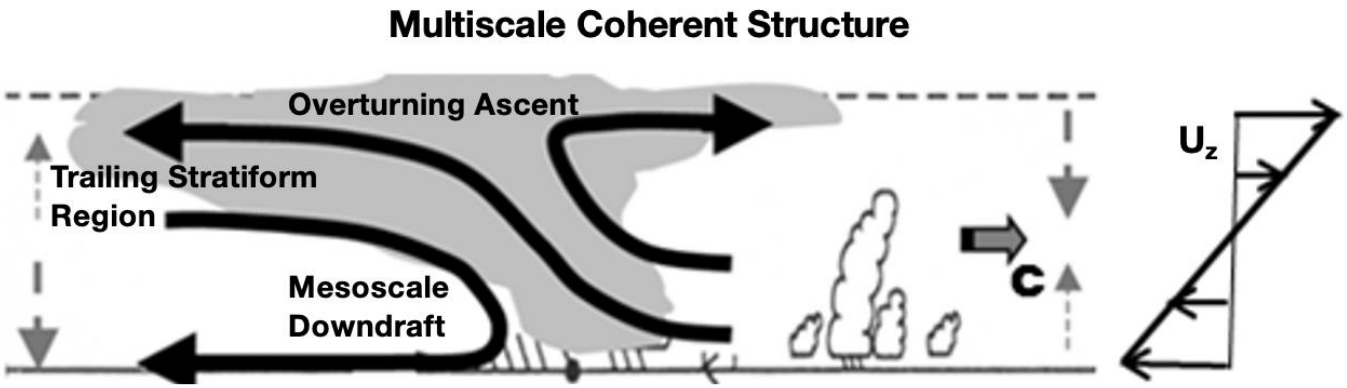

Figure 1: Diagram of multiscale coherent structure with a slantwise overturning layer including a trailing stratiform region, an overturning ascent, and a mesoscale downdraft.(adapted from MLB17) The structure is propagating from left to right at speed 'C' in a sheared wind environment depicted by 'U_z'.

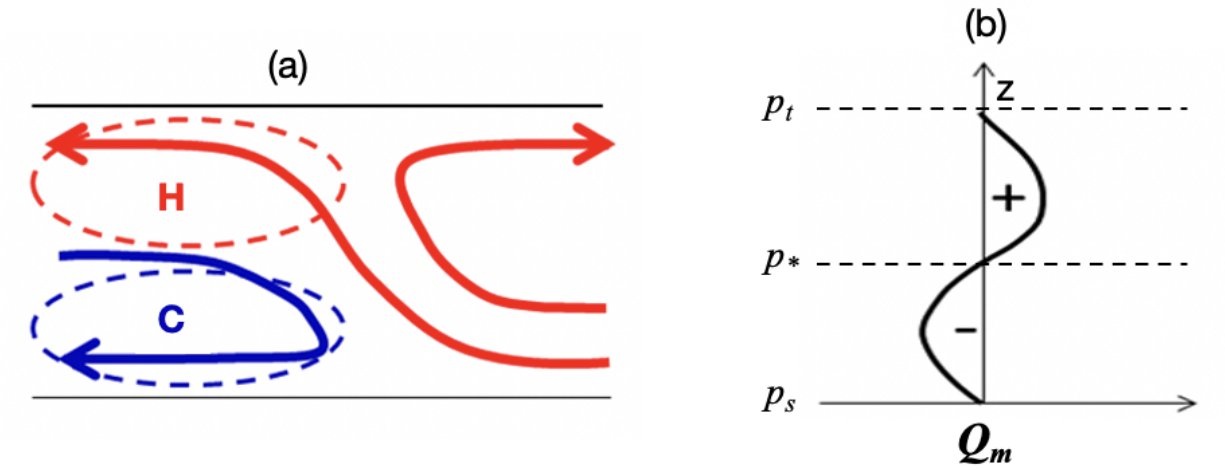

Figure 2: (a) Idealization of mesoscale heating (H) and cooling (C) regions of the prototype MSCP adopted for the prototype MCSP of Moncrieff et al. (2017). The heating/cooling dipole in (b) is consistent with the mesoscale ascent (thick red lines) and cool mesoscale descent (thick blue line) in (a). (adapted from Fig. 12 of MLB17)

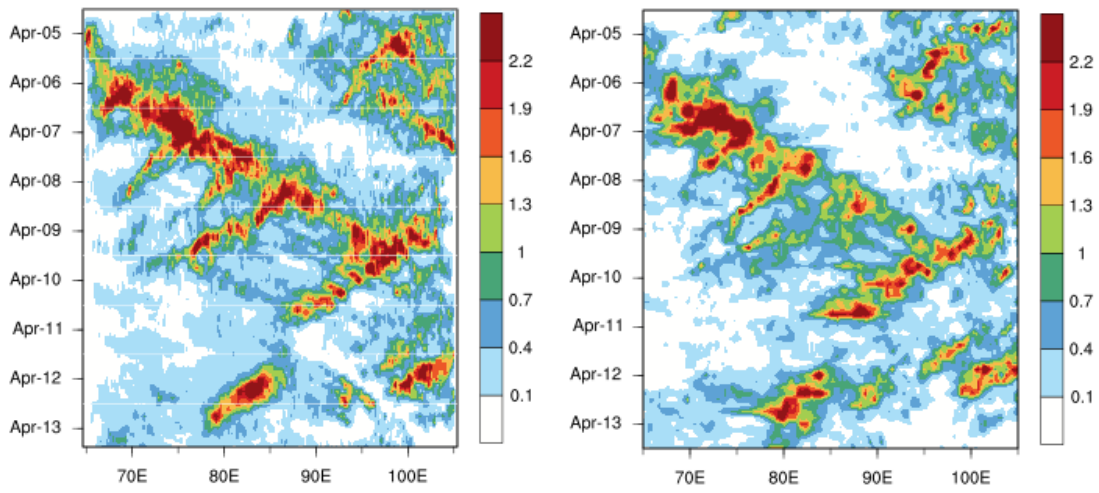

Figure 3: Observed (left) and modeled (right) time-longitude distributions of 6.5°S-6.5°N averaged hourly precipitation rate (mm h^{-1}) for 5-13 April 2009.

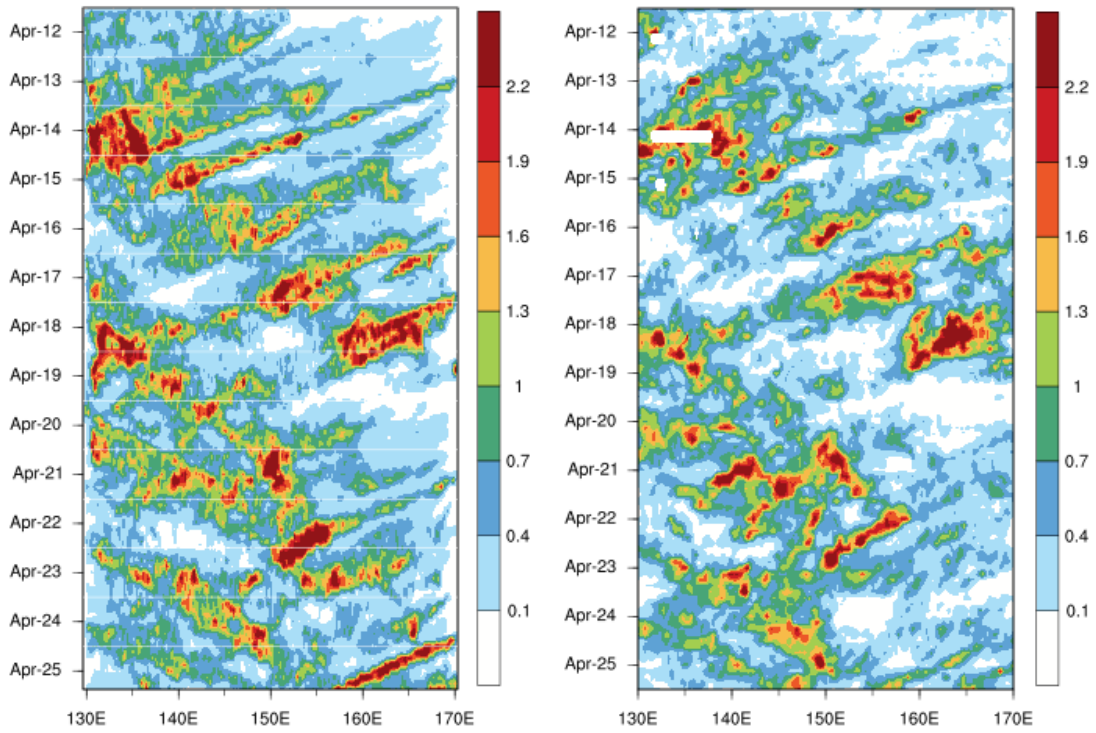

Figure 4: Observed (left) and modeled (right) time-longitude distributions of 5.5°S-7.5°N averaged hourly precipitation rate (mm h^{-1}) for 12-25 April 2009.

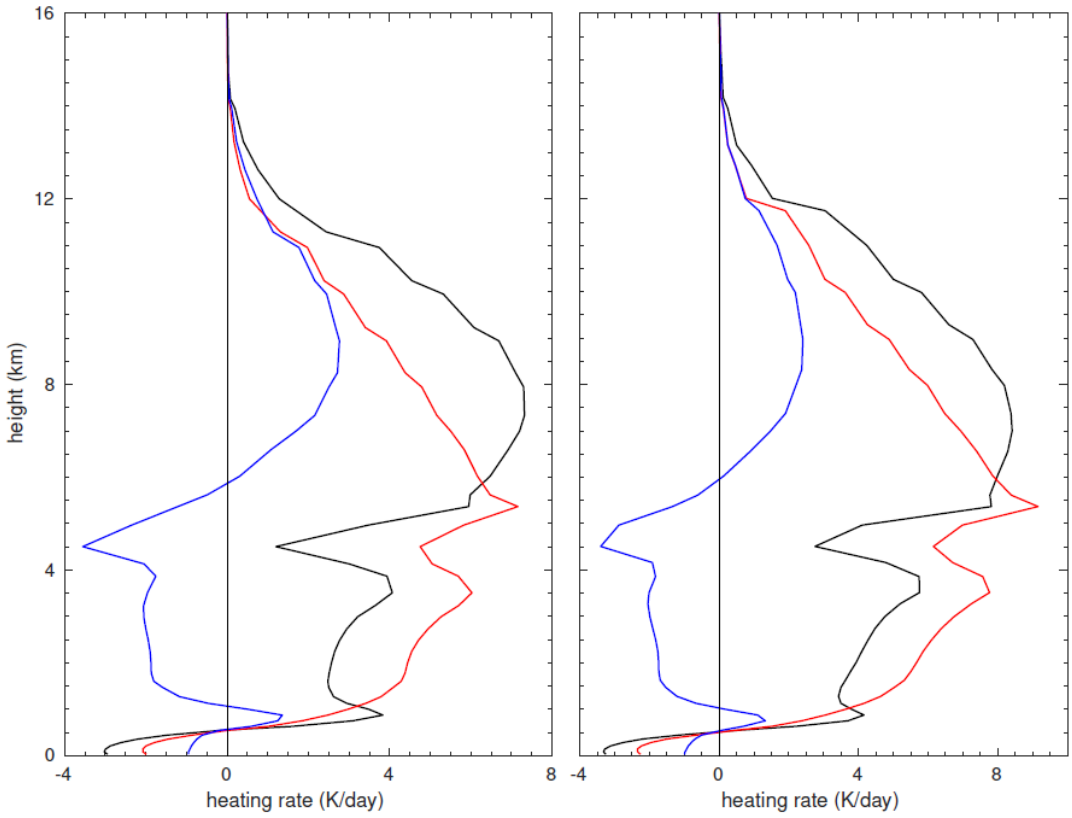

Figure 5: Heating profiles for deep convection (red), stratiform and shallow convection (blue), and their sum (black). The left and right panels are corresponding to the convective episode (5-13 April 2009) in the Indian Ocean and the convective episode (12-25 April 2009) in the western Pacific, respectively.

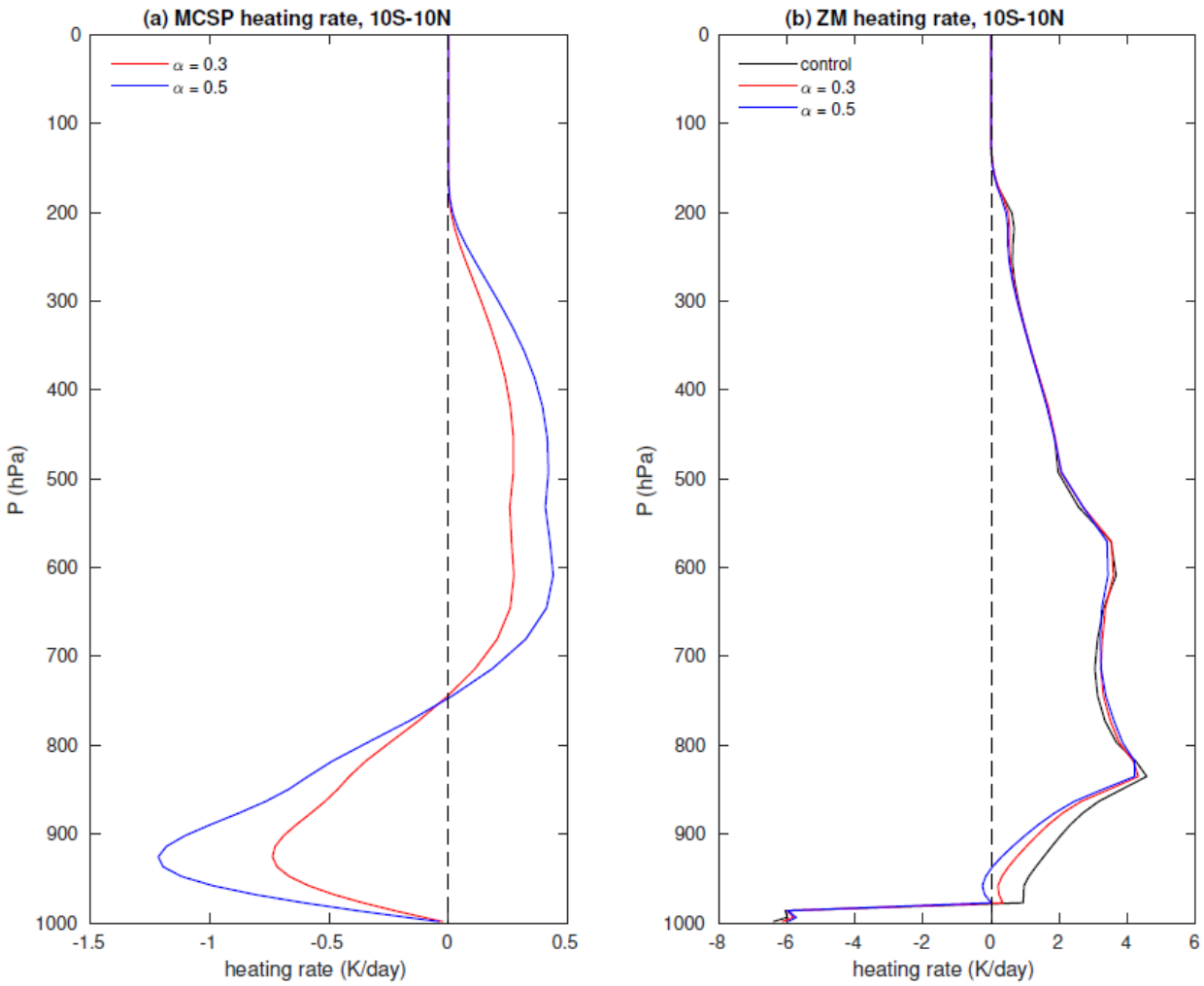

606

607 **Figure 6:** One-month (1980/11) averaged heating rate profile due to a) deep convection scheme with
608 MCSP parameterization, and b) MCSP parameterization by EAMv1 simulations.

609

610

611

612

613

614

615

616

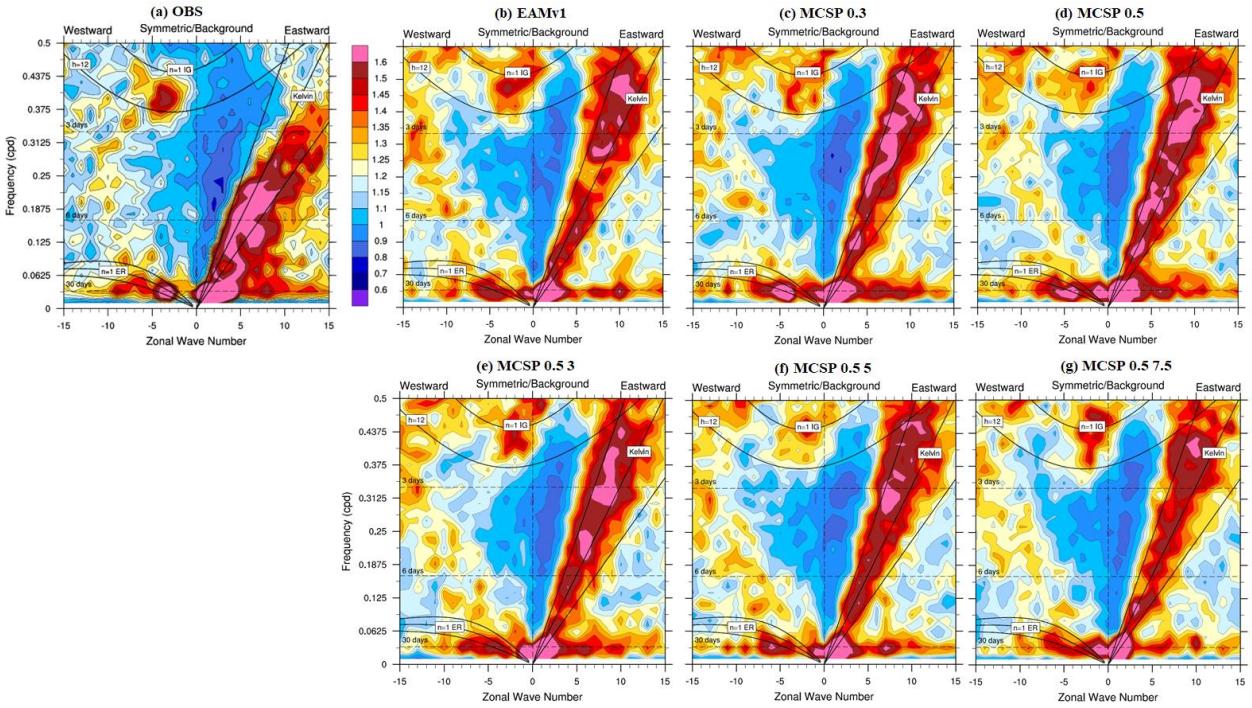

Figure 7: Symmetric component of frequency-wavenumber power spectra of precipitation based on methodology of Wheeler and Kiladis (1999) for: a) TRMM, b) baseline EAMv1 simulation, c) EAMv1 with MCSP and □ = 0.3, d) EAMv1 with MCSP and □ = 0.5, e) EAMv1 with MCSP and □ = 0.5, wind shear trigger = 3 m/s, f) EAMv1 with MCSP and □ = 0.5, wind shear trigger = 5 m/s, and g) EAMv1 with MCSP and □ = 0.5, wind shear trigger = 7.5 m/s.

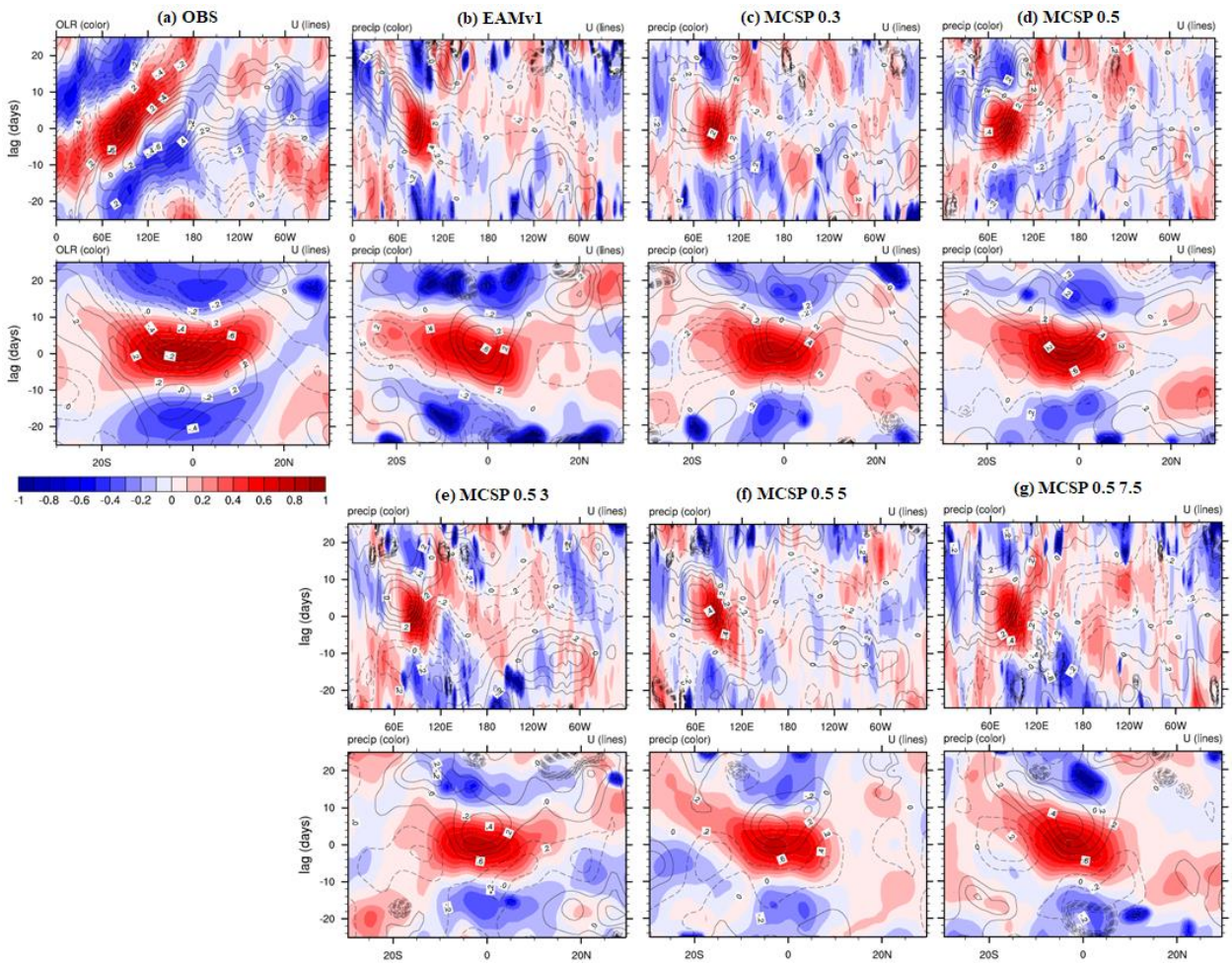

Figure 8: Cross-lag correlation of precipitation and zonal wind at 850 hPa during the boreal winter by a) ERA-Interim, and simulations by EAMv1: b) baseline model, c) MCSP with = 0.3, d) MCSP with = 0.5, e) MCSP = 0.5 and a wind shear threshold of 3 m/s, f) MCSP = 0.5 and a wind shear threshold of 5 m/s, g) MCSP = 0.5 and a wind shear threshold of 7.5 m/s.

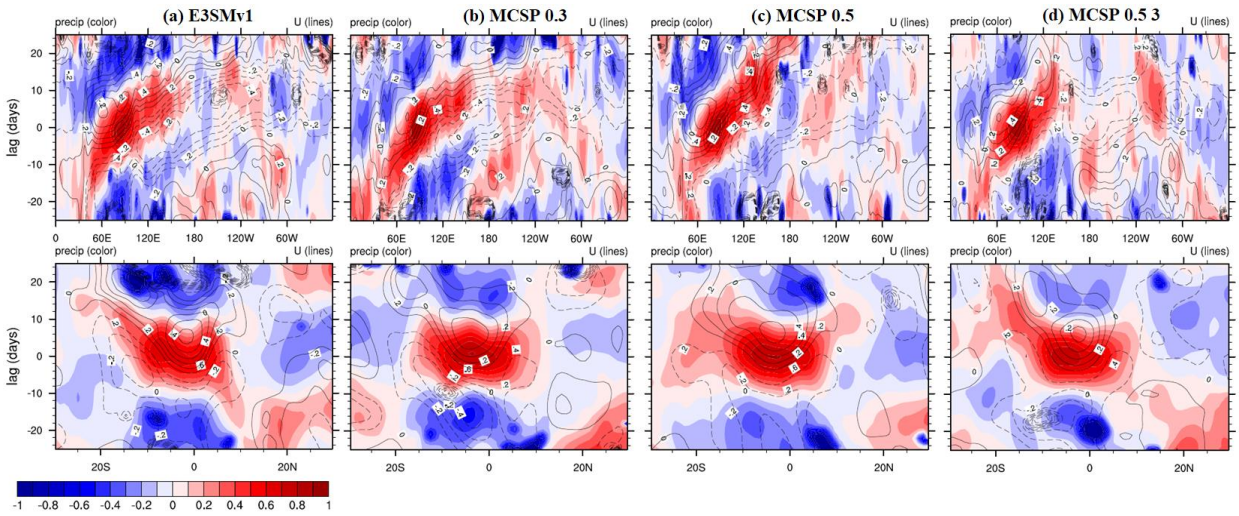

646

647 **Figure 9:** Cross-lag correlation during winter months in the northern hemisphere based on simulations of
648 E3SMv1: a) baseline model, b) MCSP □ = 0.3, c) MCSP □ = 0.5, d) MCSP □ = 0.5 and a wind shear
649 threshold of 3 m/s.

650

651

652

653

654

655

656

657

658

659

660

661

662

663

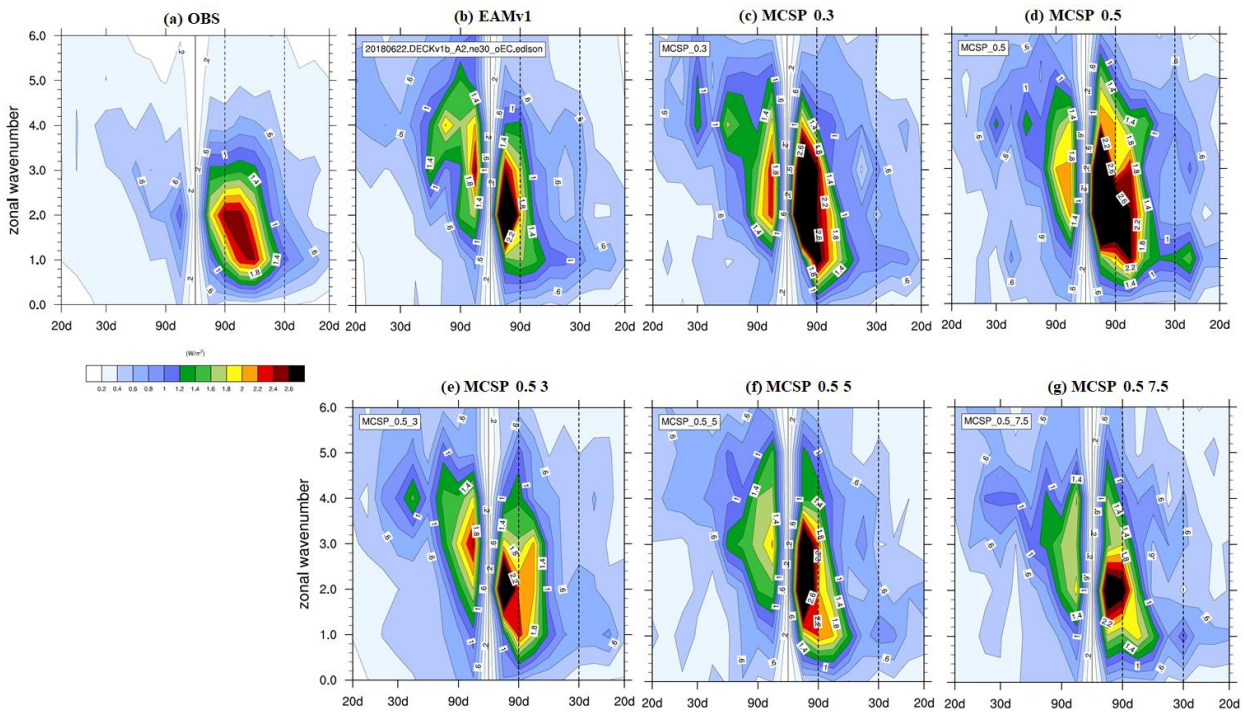

Figure 10: Same as Fig. 8, except for outgoing longwave radiation (OLR).

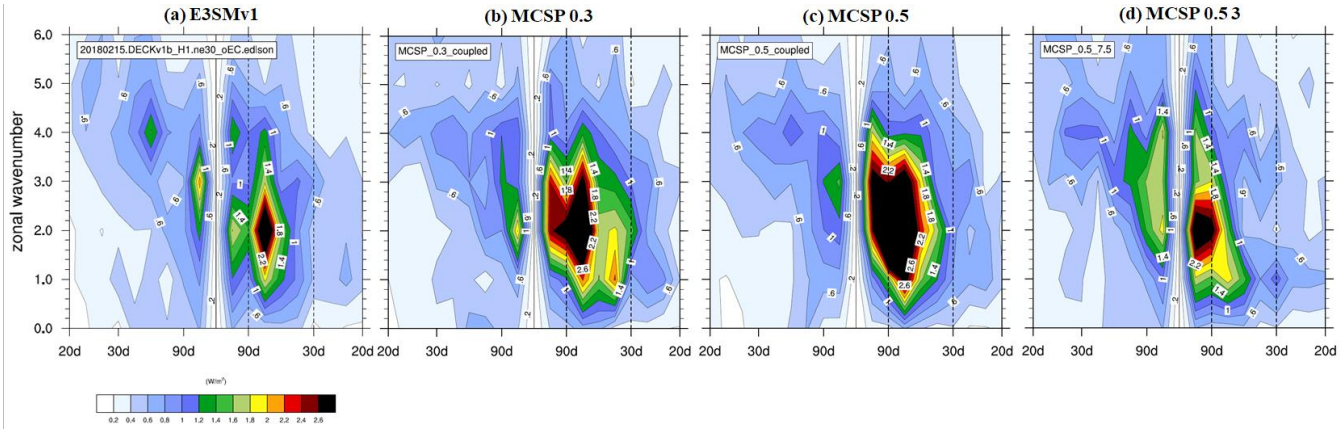

Figure 11: Same as Fig. 9, except for the spectra of OLR.

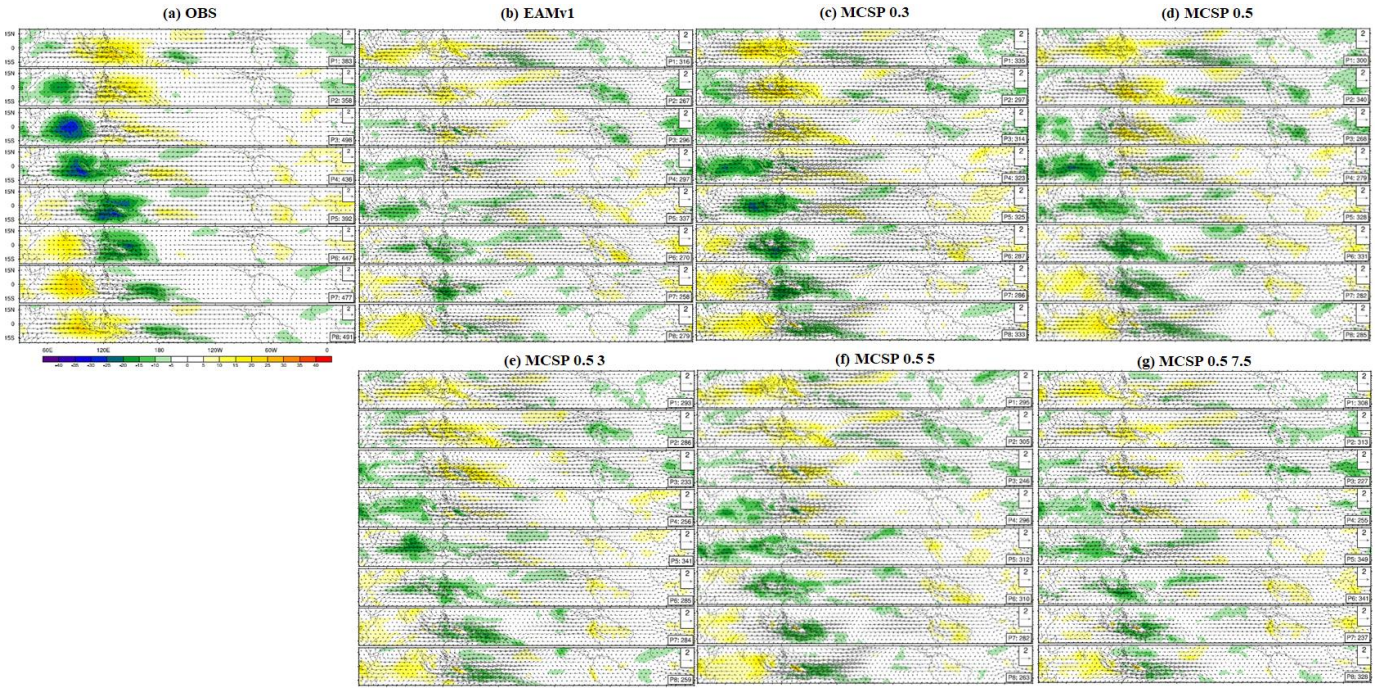

Figure 12: Life-cycle composite of MJO for the same simulations as those shown in Fig. 8.

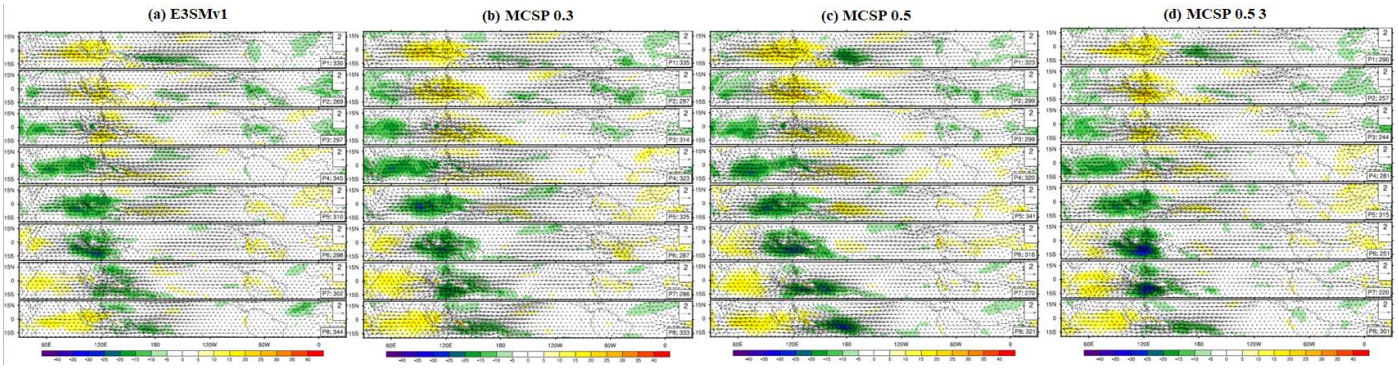

Figure 13: Life-cycle composite of MJO for the same simulations as those shown in Fig. 9.

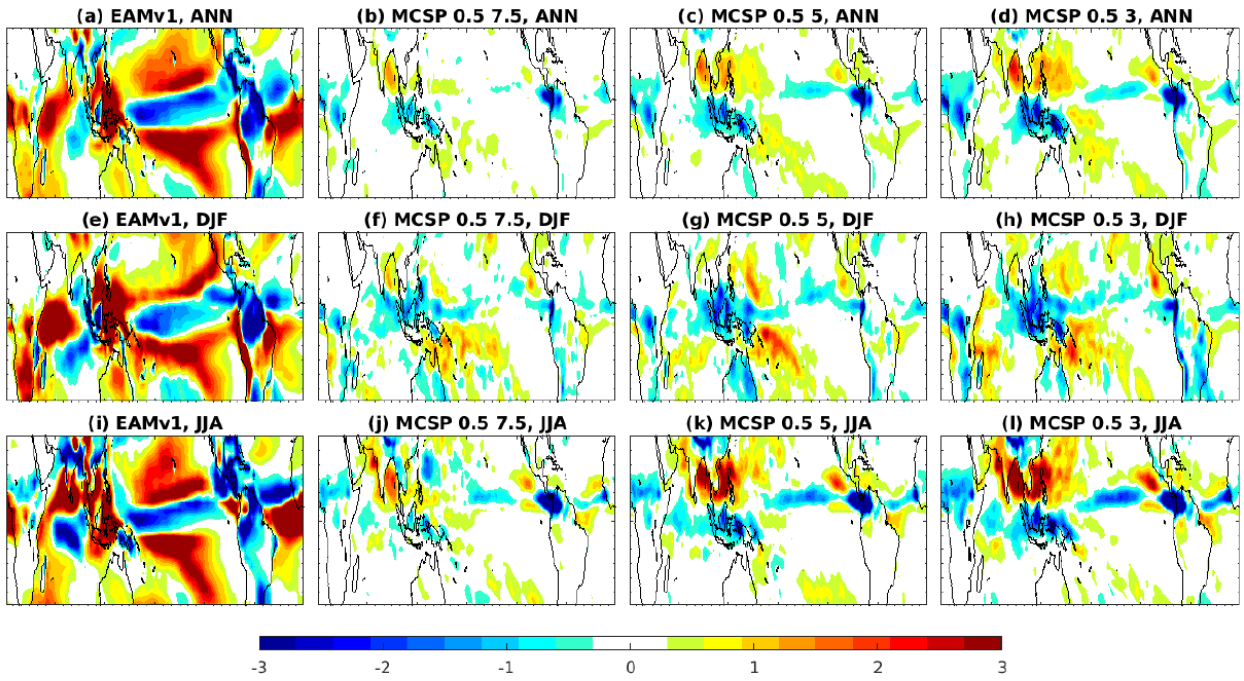

733

734 **Figure 14:** Precipitation biases (mm/day) simulated by EAMv1: 1) top panels as annual averages, 2)
735 middle panel for DJF, and 3) bottom panels for JJA. The first column is for the baseline model against
736 GPCP and the rest columns are for MCSP with various configurations against the baseline model. The
737 second column is for MCSP with □ = 0.5 and a wind shear threshold 7.5 m/s, the third column is for
738 MCSP with □ = 0.5 and a wind shear threshold 5 m/s, and the last column is for MCSP with □ = 0.5
739 and a wind shear threshold 3 m/s.

740

741

742

743

744

745

746

747

748

749

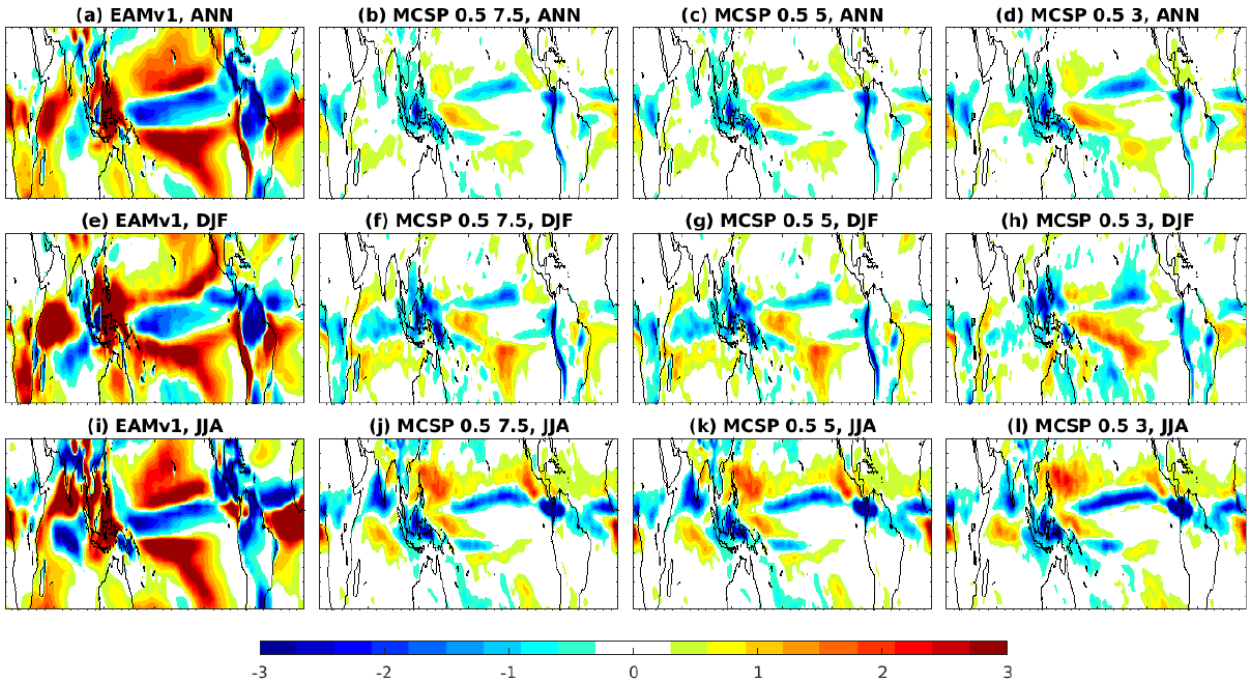

750

751 **Figure 15:** Similar as Fig. 14 but for E3SMv1 simulations. The first column is the control model
752 simulation biases against GPCP 2.3 and the rest columns are for MCSP with various configurations
753 against the baseline model. The second column is MCSP with □ = 0.3, the third column is MCSP with □
754 = 0.5, and the last column is MCSP with □ = 0.5 and a zonal wind shear trigger 3 m/s.

755